# UC Santa Barbara

## UC Santa Barbara Previously Published Works


### Title

Fermi surface nesting and the Lindhard response function in the kagome superconductor $CsV_3Sb_5$


### Permalink

https://escholarship.org/uc/item/4450m4mx



### Journal

Applied Physics Letters, 120(11)

### ISSN

0003-6951 1077-3118



### Authors

Kaboudvand, Farnaz
Teicher, Samuel M. L
Wilson, Stephen D
et al.



### Publication Date

2022-03-14

### DOI

10.1063/5.0081081

Peer reviewed



eScholarship.org Powered by the California Digital Library
University of California

# Fermi surface nesting and the Lindhard response function in the kagome superconductor $CsV_3Sb_5$

Farnaz Kaboudvand,[1, a)] Samuel M. L. Teicher,[1, a)] Stephen D. Wilson,[1] Ram Seshadri,[1] and Michelle D. Johannes[2]
[1)]*Materials Department, Materials Research Laboratory, and California NanoSystems Institute University of California Santa Barbara, California 93106, United States*
[2)]*Center for Computational Materials Science, Naval Research Laboratory, Washington, D.C. 20375, United States*

(*Electronic mail: michelle.johannes@nrl.navy.mil)

(Dated: 25 February 2022)

The recently discovered kagome net compounds $AV_3Sb_5$ ($A$ = K, Rb, Cs) become superconducting on cooling, in addition to displaying interesting topological features in the electronic structure. They also exhibit charge density wave ordering, which manifests as a breathing-mode distortion in the kagome layers. It has been suggested that such ordering derives from nesting between saddle points on the Fermi surface. In aid of the evolving understanding on this intriguing materials class, we present calculations of the Fermi surface nesting and the Lindhard susceptibility of $CsV_3Sb_5$. The breathing mode distortions appear to not display a simple link with Fermi surface nesting (FSN) and do not display the signatures of a Peierls-like transition. The FSN is agnostic to changes along $k_z$ and is only mildly impacted by small shifts of the Fermi level. The results suggesting that FSN is largely independent of specific features in the saddle point.

Compounds with kagome nets have attracted recent attention due to the interesting ground states they can display. As a consequence of their geometry and depending on the degree of electron filling, kagome materials are predicted to host a variety of instabilities associated with spin liquid states, superconductivity, charge density waves (CDW), and more.[1,2] The recently discovered non-magnetic kagome metals $AV_3Sb_5$ ($A$ = K, Rb, Cs) exhibit charge density wave and superconducting order and are predicted to host $\mathbb{Z}_2$ topological surface states.[3–5] The transitions and functionalities have been attributed to features in the electronic band structure, and, more specifically, the saddle point located at $M$, which participates in topological band inversion. Phenomenological models have long predicted 2D charge density waves in kagome metals with 3-fold rotational symmetry, also known as $3Q$ phases, due to perfect Fermi surface nesting (FSN) between $M$ points.[6–9] Such a $3Q$ charge density wave order has been detected experimentally in all members of the $AV_3Sb_5$ family.[10–16] These results have been supported by simulations[17] demonstrating the instability of the room temperature structure to 2D breathing mode distortions $q = [1/2, 1/2, 0]$, $q = [1/2, 1/2, 1/2]$ associated with phonon modes at the $M$ and $L$ points.

Aside from $3Q$ order, additional CDW distortions have been observed. Surface probes like scanning tunneling microscopy observe a unidirectional $4a_0$ stripe ordering,[10] and bulk X-ray diffraction results to date suggest either 2 or 4-fold distortions along the $c$-axis, meaning that the total $q$-vector for the bulk charge density wave may be $L$-type ($q = [1/2, 1/2, 1/2]$) or $U$-type ($q = [1/2, 1/2, 1/4]$).[12,13] This $c$-axis order may arise due to shift-stacking of the kagome planes,[18] or an in-out variation of the breathing mode[12]. While previous theoretical work makes Fermi surface nesting an obvious possible explanation for in-plane $3Q$ ordering, it is unclear whether these additional distortions could be attributed to nesting instabilities.

The crystal and electronic structures of $CsV_3Sb_5$ are presented in Fig. 1. (a) shows the room temperature structure with perfect un-distorted kagome net. The reciprocal space Brillouin zone with marked high symmetry points is presented in 1(b). There are two in-plane breathing mode candidates for the $CsV_3Sb_5$ structure, the Star of David (SoD) and the inverse Star of David (ISD) (also known as Tri-Hexagonal[12]) distortions, which are illustrated in 1(c) and (d), respectively. SoD and ISD are $M$-type distortions with $q = [1/2, 1/2, 0]$. (e) presents the electronic band structure of $CsV_3Sb_5$ with the $M$ saddle point region highlighted in green. While multiple saddle point features are expected in kagome metals and present in the band structure of $CsV_3Sb_5$,[19] the CDW instability in this compound is most commonly ascribed to the large flat saddle-point band at $E_F^{SP}$. Although there is some small discrepancy between calculations, *ab initio* simulations generally place the Fermi level above the saddle point, at $E_F^{DFT}$. Several experimental studies employing angle-resolved photoemission spectroscopy have suggested that the true Fermi level may lie slightly lower, just on or above the saddle point near $E_F^{SP}$.[4,15,19]

Although the Peierls description of nesting-driven distortions often succeeds in 1D materials,[20–22] for higher dimensional materials with 2D or 3D connectivity, this model needs to be extended. One way to understand whether the electron response can drive a Peierls phase transition is to calculate the susceptibility, $\chi(q, \omega)$, for a given electronic configuration and to use the zero frequency value of the Lindhard response function, $\chi_0(q, \omega = 0)$.[21] Previous work by Johannes and Mazin[23,24] demonstrated that Fermi surface nesting, which can be determined as divergence in the imaginary part of the Lindhard susceptibility, $\chi''(q)$, fails to prescriptively predict CDWs in a variety of 2D materials. The strongest peaks in $\chi''(q)$ often do not correspond to the true CDW $q$-vector seen in experiment, and many materials undergo no CDW transition despite the presence of strong FSN peaks. True elec-

[a)]These authors contributed equally

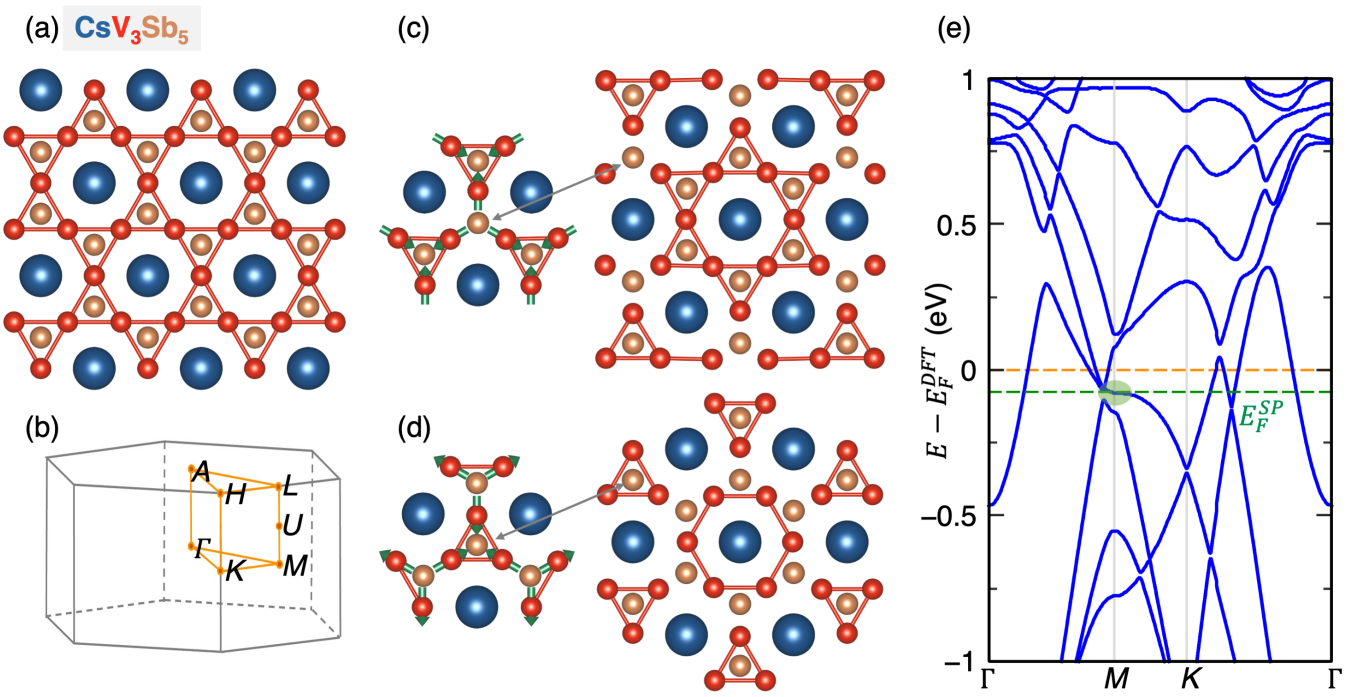


FIG. 1. Crystal and electronic structure of $CsV_3Sb_5$. (a) Room temperature structure with un-distorted kagome nets. (b) reciprocal space Brillouin zone with high symmetry points labeled. (c) and (d) present two in-plane breathing mode candidates, the Star of David (SoD) and the inverse Star of David (ISD) distortions. These $M$-type distortions have $q = [1/2, 1/2, 0]$. (e) Presents the electronic band structure of $CsV_3Sb_5$, displaying the Fermi level from DFT calculations, and the previously-observed experimental Fermi level.

tronic instability is represented instead by peaks in the real part of the susceptibility, $\chi'(q)$. A FSN-driven CDW distortion, argue Johannes and Mazin, can only be attributed to a simple Peierls-like origin if a strong Fermi surface nesting peak at the experimental $q$-vector in $\chi''$ carries over to a similar peak at the same location in $\chi'(q)$.[24] This method was demonstrated to clarify the distortion mechanism in $NbSe_2$, a quasi-2D hexagonal metal with charge density wave ($T^{CDW} \approx 35\,K$[25]) and superconducting ($T_c \approx 7.2\,K$[26]) transitions and striking behavioral similarity to quasi-2D hexagonal $CsV_3Sb_5$ ($T^{CDW} = 94\,K$, $T_c = 2.5\,K$[4]); while the $NbSe_2$ $\chi''(q)$ calculation produces a peak at $q = [1/3, 1/3, 0]$, the $\chi'$ calculation generates a completely separate peak that reproduces the experimentally-observed $q$-vector at $[1/3, 0, 0]$.[23]

Given the significant volume of qualitative discussion surrounding Fermi surface nesting in the $AV_3Sb_5$ system at present,[12,16,18,19,27–29] here we offer explicit FSN and Lindhard response calculations on $CsV_3Sb_5$ to determine whether the CDW can be attributed to a clear Peierls-like nesting mechanism.

We used the Wien2k full potential code[30] with the Perdew-Burke-Ernzerhof (PBE)[31] approximation to the exchange correlation functional. The spin-orbit interaction was accounted for using the second variational principle, as implemented in the code. We used the structure relaxed with the VASP code[32,33] where a van-der-Waals correction was added to better approximate the distance between the 2D planes (We employed the PBE functional[31] with D3 correction[34]; all parameters were identical to Ref.[4]. $a$ and $c$ unit cell parameters were 5.45 Å and 9.35 Å, respectively). We used a dense k-mesh of $20\times20\times9$ for the self-consistent calculation and then a denser mesh of $50\times50\times12$ for calculation of the Fermi surface and the real and imaginary parts of the Lindhard function, taken in both cases in the limit that the frequency goes to zero[23,24].

Our results are summarized in Fig 2. Fig 2 (a) presents $\chi''(q)$ calculated for $E_F = E_F^{DFT}$. The largest peaks correspond to the perfect self nesting at $q = [0,0]$, $q = [1,0]$, etc. and provide no real information. The additional peaks form a complex pattern of ridges. At the $M$-points, with $q$-vectors $[1/2, 0.0], [1/2, 1/2], [0.0, 1/2]$, there is indeed a peak in the nesting function. One such $q$-vector is indicated with a red arrow. However, this peak is not isolated, but instead part of a larger triangular ridge pattern that runs along the $\Gamma - M$ lines. These triangular nesting ridges have a finer grained striped texture, with up to three parallel nesting lines. A near circular nesting pattern rings the largest trivial peaks. All of these nesting features are similar for the $k_z = 0$ and $k_z = 1/2$ planes. In (b), the $\Gamma - M$ nesting ridges are shown to carry over to the real part, $\chi'(q)$. The circular ridges also have increased intensity in $\chi'(q)$. In fact, the highest intensity peaks of $\chi'(q)$ are associated with the circular ridges and do not occur at $M$-like $q$ vectors. We also performed Lindhard susceptibility calculations with the saddle point shifted to the Fermi level. The imaginary part and the real part of those calculations at different $k_z$ values are presented in Fig. 2 (c) and (d), respectively. Although the relative peak heights vary when adjusting Fermi level, there is no major qualitative difference between the Lindhard calculations.

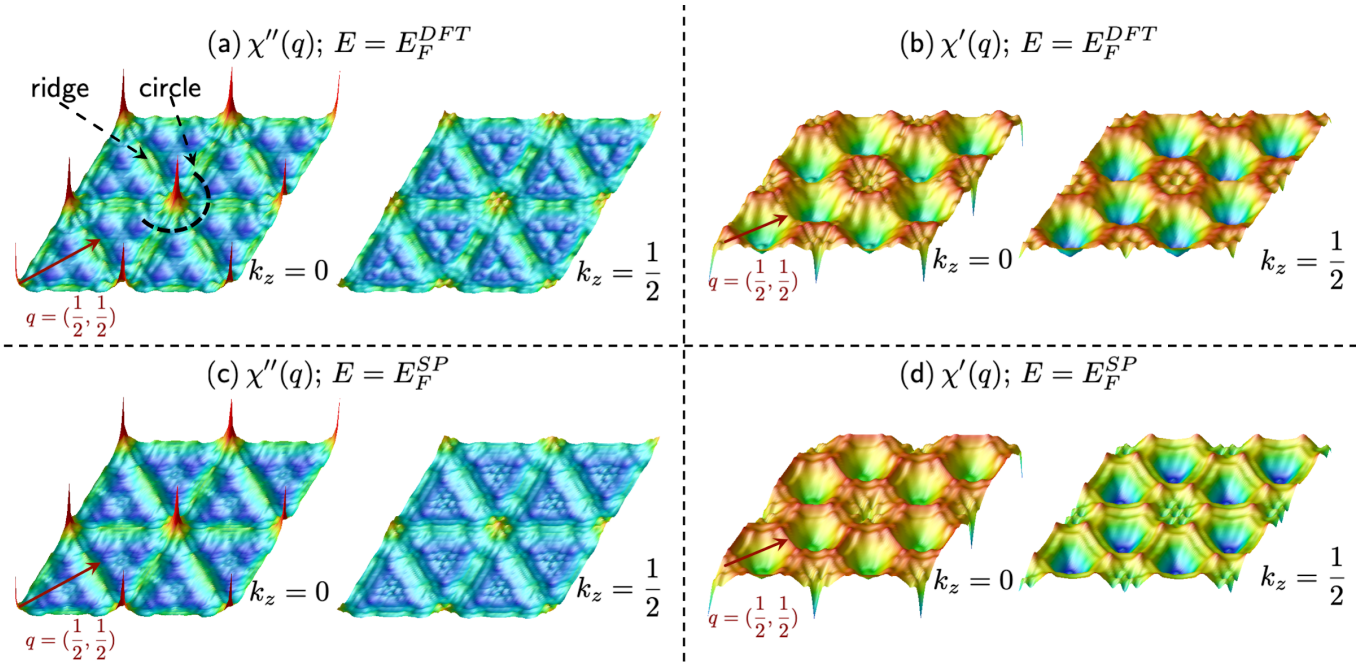


FIG. 2. Fermi surface nesting and Lindhard response function in $CsV_3Sb_5$. The imaginary and the real part of the Lindhard susceptibility function at different $k_z$ for the DFT Fermi level electronic structure is presented in (a) and (b), respectively. The imaginary and the real part at the saddle point (SP) energy level are presented in (c) and (d).

This combination of circular and triangular ridges in the Lindhard function matches the pattern previously observed in experimental quasi-particle interference measurements[10] and can be explained in terms of the Fermi surface geometry. Fig. 3 presents the Fermi surfaces calculated for both (a) $E_F^{DFT}$ and (b) $E_F^{SP}$. In both cases, the Fermi surface topography is qualitatively similar, with a central circular Fermi surface pocket surrounded with hexagonal and triangular pockets. The central pocket, which derives mainly from antimony $p$ states, nests with the larger hexagonal pocket to generate the central circular patterns in the Lindhard function. The remaining triangular and hexagonal pockets, which have primary V $d$ contributions, have strong 2D nesting of linear segments all along the $\Gamma - M$ direction, indicated by green lines. The $M$-point of this nesting is indicated with a red arrow. By contrast, the saddle-point nesting, indicated in (b), results in very small overlap and therefore does not strongly affect the overall Lindhard function.

These results allow us to make a number of statements about Fermi surface nesting-driven instabilities in $CsV_3Sb_5$ and other $AV_3Sb_5$ kagome family members (which have virtually indistinguishable electronic structure). First, the peaks at the M-point in the nesting function and real part of susceptibility are not uniquely strong, instead they are part of ridges along $\Gamma - M$. This indicates that they do not drive the electronic instability, though some contribution is not out of the question. When considering the real part of the Lindhard function, the $\Gamma - M$ ridges have intensity similar to or less than the central circular ridge that arises due to nesting of the central pocket of the Fermi surface, which originates primarily from the Sb $p$, with the somewhat larger hexagonal pocket. Second, Fermi surface nesting is $k_z$ agnostic. Despite small changes in the magnitude of the peaks, the $\chi''(q)$ and $\chi'(q)$ maps are qualitatively identical at $k_z = 0$ and $k_z = 1/2$ for all calculations. This is true not just for high symmetry planes; e.g., the results for $k_z = 1/4$ are also similar. It is therefore difficult to argue that either the 2-fold or 4-fold $c$-axial distortions seen in experiment could be uniquely favored by electronic structure instability. Finally, because the Lindhard function is not altered appreciably with changing Fermi level and/or at different $k_z$ value (the $M$ saddle point is at $k_z = 0$), the kagome saddle point appears to be irrelevant to the total nesting. In fact, the Lindhard intensity does not even favor V kagome intrinsic instability related to outer pockets of the Fermi surface over instability involving the central circular antimony pocket.

Zhu *et al.*[22] proposed a classification of CDWs into three different types based on the mechanism behind their formation. Within this scheme, type-I CDWs follow the Peierls picture—wherein the transition is driven by FSN, whereas type-II CDWs are associated with q-dependent electron–phonon coupling, and type-III covers correlated systems with charge modulations such as cuprates in which neither FSN nor electron-phonon coupling appear to explain the transition. Overall, our results support the view that the charge density waves in $CsV_3Sb_5$ do not derive from a unique instability in the electronic structure and cannot be categorized as type-I Peierls-like distortions. Electron-phonon coupling has been identified as the main driver of structural instability in $NbSe_2$[23,35] and is a likely explanation of the observed ordering in the $AV_3Sb_5$ family as well. While new experiments indicate that the phonon transitions in $CsV_3Sb_5$[36,37]

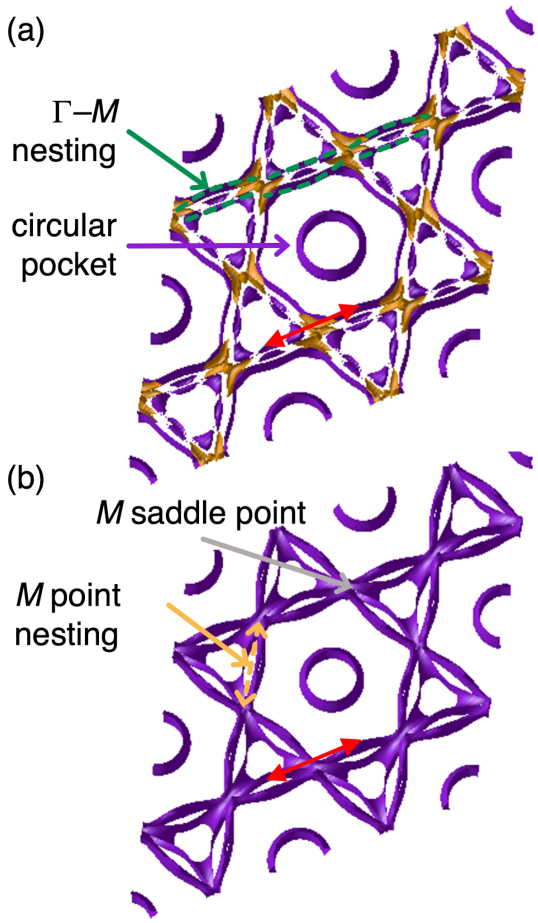


FIG. 3. Fermi surfaces and origins of nesting. Fermi surfaces are presented at (a) $E_F^{DFT}$ (b) $E_F^{SP}$. The circular FSN ridges derive from nesting between central circular and hexagonal pockets. The $\Gamma - M$ FSN ridges derive from strong nesting and linear overlap of the triangular and hexagonal regions, highlighted in green. The main $M$-type FSN vector is highlighted in red for both Fermi level choices, while the weak saddle point nesting at the $M$-point is indicated in orange in (b). The Figure illustrates that they are multiple type of M-like nesting that we could have in this Fermi surface, and the dominant M-type nesting is not the one between the M saddle points (M point nesting which showed by the orange dashed arrow is not the dominant nesting). The saddle point shows up in Fermiology as extremely 2-D rectangles oriented such the nesting is weak (if even existed).

may be more complex than the phonon softening previously observed in $NbSe_2$, electron phonon-coupling effects may explain the strong influence of chemical doping on the CDW in this compound[38,39]. Although we have demonstrated that the $M$ saddle point does not play a major role in Fermi surface nesting, the peak in the density of states associated with the saddle-point, a van Hove singularity, may still play an essential role in the CDW transition. Van Hove singularities have long been known to contribute to anomalies in the elastic properties[40] and phonon spectra[41] of metals and the proximity of van Hove singularities to the Fermi level can still govern the magnitude of phonon hardening or softening even in systems where the CDW $q$ vector can be derived from Fermi surface nesting[42].

This work was supported by the National Science Foundation (NSF) through Enabling Quantum Leap: Convergent Accelerated Discovery Foundries for Quantum Materials Science, Engineering and Information (Q-AMASE-i): Quantum Foundry at UC Santa Barbara (DMR-1906325). We acknowledge use of the shared computing facilities of the Center for Scientific Computing at UC Santa Barbara, supported by NSF CNS-1725797, and the NSF MRSEC at UC Santa Barbara, NSF DMR-1720256. FK acknowledges the Roy T. Eddleman Center for Quantum Innovation (ECQI) for their support. SMLT. has been supported by the National Science Foundation Graduate Research Fellowship Program under Grant No. DGE-1650114. MDJ acknowledges support by the Office of Naval Research through the U.S. Naval Research Laboratory.

## I. REFERENCES

[1]H.-M. Guo and M. Franz, "Topological insulator on the kagome lattice," *Phys. Rev. B*, vol. 80, p. 113102, 2009.
[2]W.-H. Ko, P. A. Lee, and X.-G. Wen, "Doped kagome system as exotic superconductor," *Phys. Rev. B*, vol. 79, p. 214502, 2009.
[3]B. R. Ortiz, L. C. Gomes, J. R. Morey, M. Winiarski, M. Bordelon, J. S. Mangum, I. W. Oswald, J. A. Rodriguez-Rivera, J. R. Neilson, S. D. Wilson, , E. Ertekin, T. M. McQueen, and E. S. Toberer, "New kagome prototype materials: discovery of $KV_3Sb_5$, $RbV_3Sb_5$, and $CsV_3Sb_5$," *Phys. Rev. Mater.*, vol. 3, p. 094407, 2019.
[4]B. R. Ortiz, S. M. L. Teicher, Y. Hu, J. L. Zuo, P. M. Sarte, E. C. Schueller, A. M. Abeykoon, M. J. Krogstad, S. Rosenkranz, R. Osborn, R. Seshadri, L. Balents, J. He, and S. D. Wilson, "$CsV_3Sb_5$: A $\mathbb{Z}_2$ topological kagome metal with a superconducting ground state," *Phys. Rev, Lett.*, vol. 125, p. 247002, 2020.
[5]B. R. Ortiz, E. Kenney, P. M. Sarte, S. M. L. Teicher, R. Seshadri, M. J. Graf, and S. D. Wilson, "Superconductivity in the $\mathbb{Z}_2$ kagome metal $KV_3Sb_5$," *Phys. Rev. Materials*, vol. 5, p. 034801, 2020.
[6]T. Park, M. Ye, and L. Balents, "Electronic instabilities of kagome metals: Saddle points and Landau theory," *Phys. Rev. B*, vol. 104, p. 035142, 2021.
[7]R. Nandkishore, G.-W. Chern, and A. V. Chubukov, "Itinerant half-metal spin-density-wave state on the hexagonal lattice," *Phys. Rev. Lett.*, vol. 108, p. 227204, 2012.
[8]R. Nandkishore and A. V. Chubukov, "Interplay of superconductivity and spin-density-wave order in doped graphene," *Phys. Rev. B*, vol. 86, p. 115426, 2012.
[9]W.-S. Wang, Z.-Z. Li, Y.-Y. Xiang, and Q.-H. Wang, "Competing electronic orders on kagome lattices at van hove filling," *Phys. Rev. B*, vol. 87, p. 115135, 2013.
[10]H. Zhao, H. Li, B. R. Ortiz, S. M. L. Teicher, T. Park, M. Ye, Z. Wang, L. Balents, S. D. Wilson, and I. Zeljkovic, "Cascade of correlated electron states in a kagome superconductor $CsV_3Sb_5$," *Nature*, 2021.
[11]Y.-X. Jiang, J.-X. Yin, M. M. Denner, N. Shumiya, B. R. Ortiz, G. Xu, Z. Guguchia, J. He, M. S. Hossain, X. Liu, J. Ruff, L. Kautzsch, S. S. Zhang, G. Chang, I. Belopolski, Q. Zhang, T. A. Cochran, D. Multer, M. Litskevich, Z.-J. Cheng, X. P. Yang, Z. Wang, R. Thomale, T. Neupert, S. D. Wilson, and M. Z. Hasan, "Unconventional chiral charge order in kagome superconductor $KV_3Sb_5$," *Nat. Mater.*, vol. 20, pp. 1353–1357, 2021.
[12]B. R. Ortiz, S. M. Teicher, L. Kautzsch, P. M. Sarte, J. P. Ruff, R. Seshadri, and S. D. Wilson, "Fermi surface mapping and the nature of charge density wave order in the kagome superconductor $CsV_3Sb_5$," *arXiv preprint arXiv:2104.07230*, 2021.
[13]H. Miao, H. Li, H. Lee, A. Said, H. Lei, J. Yin, M. Hasan, Z. Wang, H. Tan, and B. Yan, "Geometry of the charge density wave in kagomé metal $AV_3Sb_5$," *arXiv preprint arXiv:2106.10150*, 2021.
[14]Z. Liu, N. Zhao, Q. Yin, C. Gong, Z. Tu, M. Li, W. Song, Z. Liu, D. Shen, Y. Huang, K. Liu, H. Lei, and S. Wang, "Charge-density-wave-

induced bands renormalization and energy gaps in a kagome superconductor $RbV_3Sb_5$," *Phys. Rev. X*, vol. 11, p. 041010, 2021.

[15] Y. Hu, S. M. L. Teicher, B. R. Ortiz, Y. Luo, S. Peng, L. Huai, J. Ma, N. Plumb, S. D. Wilson, J.-F. He, and M. Shi, "Charge-order-assisted topological surface states and flat bands in the kagome superconductor $CsV_3Sb_5$," *arXiv preprint arXiv:2104.12725*, 2021.

[16] H. Luo, Q. Gao, H. Liu, Y. Gu, D. Wu, C. Yi, J. Jia, S. Wu, X. Luo, Y. Xu, L. Zhao, Q. Wang, H. Mao, G. Liu, Z. Zhu, Y. Shi, K. Jiang, J. Hu, Z. Xu, and X. J. Zhao, "Electronic nature of charge density wave and electron-phonon coupling in kagome superconductor $KV_3Sb_5$," *arXiv preprint arXiv:2107.02688*, 2021.

[17] H. Tan, Y. Liu, Z. Wang, and B. Yan, "Charge density waves and electronic properties of superconducting kagome metals," *Phys. Rev. Lett.*, vol. 127, p. 046401, 2021.

[18] N. Ratcliff, L. Hallett, B. R. Ortiz, S. D. Wilson, and J. W. Harter, "Coherent phonon spectroscopy and interlayer modulation of charge density wave order in the kagome metal $CsV_3Sb_5$," *arXiv preprint arXiv:2104.10138*, 2021.

[19] M. Kang, S. Fang, J.-K. Kim, B. R. Ortiz, J. Yoo, B.-G. Park, S. D. Wilson, J.-H. Park, and R. Comin, "Twofold van hove singularity and origin of charge order in topological kagome superconductor $CsV_3Sb_5$," *arXiv preprint arXiv:2105.01689*, 2021.

[20] R. E. Peierls, *Quantum theory of solids*. Clarendon Press, 1996.

[21] X. Zhu, J. Guo, J. Zhang, and E. Plummer, "Misconceptions associated with the origin of charge density waves," *Adv. Phys. X*, vol. 2, pp. 622–640, 2017.

[22] X. Zhu, Y. Cao, J. Zhang, E. Plummer, and J. Guo, "Classification of charge density waves based on their nature," *Proc. Natl. Acad. Sci. U.S.A.*, vol. 112, pp. 2367–2371, 2015.

[23] M. Johannes, I. Mazin, and C. Howells, "Fermi-surface nesting and the origin of the charge-density wave in $NbSe_2$," *Phys. Rev. B*, vol. 73, p. 205102, 2006.

[24] M. Johannes and I. Mazin, "Fermi surface nesting and the origin of charge density waves in metals," *Phys. Rev. B*, vol. 77, p. 165135, 2008.

[25] D. E. Moncton, J. D. Axe, and F. J. DiSalvo, "Study of superlattice formation in $2H$-$NbSe_2$ and $2H$-$TaSe_2$ by neutron scattering," *Phys. Rev. Lett.*, vol. 34, pp. 734–737, 1975.

[26] J. M. E. Harper, T. H. Geballe, and F. J. Di Salvo, "Heat capacity of $2H$-$NbSe_2$ at the charge density wave transition," *Phys. Lett. A*, vol. 54, pp. 27–28, 1975.

[27] Y.-P. Lin and R. M. Nandkishore, "Complex charge density waves at van hove singularity on hexagonal lattices: Haldane-model phase diagram and potential realization in kagome metals $AV_3Sb_5$," *arXiv preprint arXiv:2104.02725*, 2021.

[28] R. Lou, A. Fedorov, Q. Yin, A. Kuibarov, Z. Tu, C. Gong, E. F. Schwier, B. Büchner, H. Lei, and S. Borisenko, "Charge-density-wave-induced peak-dip-hump structure and flat band in the kagome superconductor $CsV_3Sb_5$," *arXiv preprint arXiv:2106.06497*, 2021.

[29] C. Wang, S. Liu, H. Jeon, and J.-H. Cho, "Origin of charge density wave in layered kagome metal $CsV_3Sb_5$," *arXiv preprint arXiv:2109.01921*, 2021.

[30] P. Blaha, K. Schwarz, G. Madsen, D. Kvasnicka, and J. Luitz, *WIEN2K: An Augmented Plane Wave and Local Orbitals Program for Calculating Crystal Properties*. Karlheinz Schwarz, 2001.

[31] J. P. Perdew, K. Burke, and M. Ernzerhof, "Generalized gradient approximation made simple," *Phys. Rev. Lett.*, vol. 77, p. 3865, 1996.

[32] P. E. Blöchl, "Projector augmented-wave method," *Phys. Rev. B*, vol. 50, pp. 17953–17979, 1994.

[33] G. Kresse and J. Hafner, "Norm-conserving and ultrasoft pseudopotentials for first-row and transition elements," *J. Phys. Condens. Matter*, vol. 6, p. 8245, 1994.

[34] S. Grimme, S. Ehrlich, and L. Goerigk, "Effect of the damping function in dispersion corrected density functional theory," *J. Comput. Chem.*, vol. 32, no. 7, pp. 1456–1465, 2011.

[35] F. Weber, S. Rosenkranz, J.-P. Castellan, R. Osborn, R. Hott, R. Heid, K.-P. Bohnen, T. Egami, A. Said, and D. Reznik, "Extended phonon collapse and the origin of the charge-density wave in 2H-$NbSe_2$," *Phys. Rev. Lett*, vol. 107, no. 10, p. 107403, 2011.

[36] Y. Xie, Y. Li, P. Bourges, A. Ivanov, Z. Ye, J.-X. Yin, M. Z. Hasan, A. Luo, Y. Yao, Z. Wang, G. Xu, and P. Dai, "Electron-phonon coupling in the charge density wave state of $CsV_3Sb_5$," *arXiv preprint arXiv:2111.00654*, 2021.

[37] E. Uykur, B. Ortiz, S. Wilson, M. Dressel, and A. Tsirlin, "Optical detection of charge-density-wave instability in the non-magnetic kagome metal $KV_3Sb_5$," *arXiv preprint arXiv:2103.07912*, 2021.

[38] Y. M. Oey, B. R. Ortiz, F. Kaboudvand, J. Frassineti, E. Garcia, S. Sanna, V. Mitrović, R. Seshadri, and S. D. Wilson, "Fermi level tuning and double-dome superconductivity in the kagome metals $CsV_3Sb_{5-x}Sn_x$," *arXiv preprint arXiv:2110.10912*, 2021.

[39] Y. Liu, Y. Wang, Y. Cai, Z. Hao, X.-M. Ma, L. Wang, C. Liu, J. Chen, L. Zhou, J. Wang, S. Wang, H. He, Y. Liu, S. Cui, J. Wang, B. Huang, C. Chen, and J.-W. Mei, "Doping evolution of superconductivity, charge order and band topology in hole-doped topological kagome superconductors $Cs(V_{1-x}Ti_x)_3Sb_5$," *arXiv preprint arXiv:2110.12651*, 2021.

[40] V. G. Vaks and A. V. Trefilov, "The effect of proximity of the Fermi level to singularities in the electron state density on elastic and thermodynamic properties of metals and alloys," *J. of Phys. F: Met. Phys.*, vol. 18, pp. 213–235, feb 1988.

[41] L. Dagens, "Phonon anomaly near a Fermi surface topological transition," *J. Phys. F: Met. Phys.*, vol. 8, pp. 2093–2113, 1978.

[42] I. I. Naumov and O. I. Velikokhatniy, "Simultaneous manifestations of the 2D van Hove singularity and the Fermi surface nesting in the acoustic soft phonon mode of alloys," *J. Phys. Condens. Matter*, vol. 9, p. 10339, 1997.